Potential energies for Ca_2^+: Cross sections for collisions of Ca^+ and Rydberg Ca^{**} with Ca

B. Liu
IBM Research Laboratory, Monterey and Cottle Roads, San Jose, California 95197

R. E. Olson
Molecular Physics Laboratory, SRI International, Menlo Park, California 94025

(Received 24 April 1978)

Ab initio self-consistent-field (SCF) and configuration interaction (CI) calculations have yielded potential energy curves for the lowest $^2\Sigma_u^+$ and $^2\Sigma_g^+$ states of Ca_2^+. The best CI calculation yields the following parameters for the $^2\Sigma_u^+$ state: $D_e = 1.04$ eV, $R_e = 7.55a_0$, $\omega_e = 119$ cm^{-1}, and $B_e = 0.0526$ cm^{-1}. The long-range regions of the $^2\Sigma_u^+$ and $^2\Sigma_g^+$ potential curves are both characterized by a Ca dipole polarizability of $170.4a_0^3$, in good agreement with the experimental value of $(169 \pm 17)a_0^3$. The charge-transfer total cross sections have been calculated over the energy range $E_{cm} = 10$–10000 eV and are well reproduced by the functional form $Q^{1/2}(\text{Å}) = 15.67 - 3.276 \log_{10} E_{cm}$ (eV). The elastic differential-scattering rainbow angle is predicted to be located at $E\theta_R \approx 90$ eV deg. Collisional-ionization cross sections and rates were also estimated for Rydberg-atom Ca** + ground-state Ca collisions. The reaction rates are predicted to be on the order of 10^{-10} cm^3/sec and depend linearly on the principal quantum number n of the Rydberg atom.

I. INTRODUCTION

Very little is known experimentally or theoretically about the lowest $^2\Sigma_u^+$ and $^2\Sigma_g^+$ states of Ca_2^+. Spectroscopic information is lacking and the only available theoretical information is the asymptotic splitting between the $^2\Sigma_u^+$ and $^2\Sigma_g^+$ states presented by Sinha and Bardsley.[1] However, spectroscopic information is available on the low-lying excited states of Ca_2 indicating that they are excimer states similar to that observed in the rare gases.[2] Balfour and Whitlock[3] have presented an RKR analysis for the $A\,^1\Sigma_u^+$ state of Ca_2 that indicates it is bound by approximately 0.75 eV at an equilibrium separation of $7.2a_0$. By analogy with the potentials of the rare gases, we could predict a similar shape for the potential curve of the lowest $^2\Sigma_u^+$ state of Ca_2^+. Calculations by Stevens and Krauss[4] on the Mg_2^+ system further reinforce this prediction.

Thus the motivation for this study is to provide accurate *ab initio* potential energies for the two lowest states of Ca_2^+. Using these *ab initio* potential curves, we have calculated the total cross sections for charge exchange and predicted the location of the differential scattering rainbow angle. Also, we have used the information obtained from the long-range portions of the Ca_2^+ molecular states to provide estimates of the chemi-ionization cross sections for collisions between Rydberg and ground-state Ca atoms.

II. ELECTRONIC WAVE FUNCTIONS AND POTENTIAL ENERGY CURVES

A. Calculations

Electronic wave functions and potential energy curves were calculated for the lowest $^2\Sigma_u^+$ and $^2\Sigma_g^+$ states of Ca_2^+ using both the analytical expansion restricted Hartree-Fock (RHF) and the configuration interaction (CI) methods. In the CI calculation the electronic wave function was expanded in an orthonormal, n-particle basis set of $D_{\infty h}$ symmetry- and equivalence-restricted configuration state functions (CSF). These CSF were linear combinations of Slater determinants such that each had the symmetry and multiplicity of the molecular state under consideration. The spatial orbitals in the Slater determinants were expanded in terms of an elementary basis set of Slater-type functions (STF).

The elementary basis set used in this study is shown in Table I. The Ca basis set of Clementi and Roetti[5] was augmented by two $4p$ functions and three $3d$ functions. The exponents for the $4p$ functions were optimized for the self-consistent-field (SCF) energy of $Ca(4s4p, {}^3P)$, and those of the $3d$ functions were optimized for $Ca(4s3d, {}^3D)$. These

TABLE I. Slater basis set for Ca.

nl	$\delta(a_0^{-1})$	nl	$\delta(a_0^{-1})$
$1s$	19.9731	$2p$	9.12915
$1s$	32.1500	$2p$	15.9947
$2s$	17.2394	$3p$	7.37779
$2s$	8.40361	$3p$	3.62974
$3s$	7.46907	$3p$	2.34862
$3s$	3.95936	$3p$	1.64038
$3s$	3.01657	$4p$	1.0942
$4s$	3.09105	$4p$	0.6977
$4s$	1.62884	$3d$	4.76666
$4s$	1.01203	$3d$	2.1222
$4s$	0.66733	$3d$	0.8007

 © 1978 The American Physical Society

added functions provide the flexibility needed to describe the polarization of the Ca atom in an electrostatic field, and allow for the distortion of the atoms in the molecule. The final basis set yielded SCF energies of −676.758 043 and −676.569 769 hartrees for the ground states of Ca and Ca^+, respectively. These energies compare well with Clementi and Roetti's[5] results of −676.758 03 and −676.569 89 hartrees, which were near the RHF limit.

The SCF wave functions for Ca_2^+ are

$$\text{(core)}\ 6\sigma_g^2 6\sigma_u\ {}^2\Sigma_u^+$$

and

$$\text{(core)}\ 6\sigma_g 6\sigma_u^2\ {}^2\Sigma_g^+,$$

where

$$\text{(core)} = 1\sigma_g^2 \cdots 5\sigma_g^2 1\sigma_u^2 \cdots 5\sigma_u^2 1\pi_u^4 2\pi_u^4 1\pi_g^4 2\pi_g^4. \qquad (1)$$

Both wave functions dissociate formally to properly symmetrized products of single-CSF wave functions of $Ca(4s^2, {}^1S)$ and $Ca^+(4s, {}^2S)$. These single-CSF atomic wave functions are not SCF wave functions, since a common set of spatial orbitals is used to describe both Ca and Ca^+. The SCF energy of Ca_2^+ at $R=\infty$ is, for both states, −1353.323 35 hartrees as compared with the sum of the corresponding atomic SCF energies of −1353.327 81 hartrees. Therefore, the error introduced by the common-orbital restriction is quite insignificant, and, for all practical purposes, the SCF wave functions of Ca_2^+ may be considered to possess the correct formal dissociation behavior.

In the CI calculations the CSF were constructed from the occupied and virtual orbitals of the SCF calculations. Three disjoint n-particle spaces were examined: (i) the internal space spanned by all the CSF constructed solely from occupied orbitals; (ii) the singly excited space spanned by all the CSF with only one electron in a virtual orbital; and (iii) the doubly excited space spanned by all the CSF with only two electrons in virtual orbitals. From each of these n-particle spaces several subspaces were considered. Their definitions were based on a division of the occupied orbitals into the core, inner, and valence orbitals. The core orbitals were the 1σ, 2σ, 3σ, and 1π orbitals correlating with the K- and L-shell orbitals of the separated atoms; the inner orbitals were the 4σ, 5σ, and 2π orbitals correlating with the atomic M-shell orbitals; and the valence orbitals were the 6σ orbitals correlating with the $4s$ orbitals of the separated atoms. A subspace spanned by all the CSF with fully occupied core and inner orbitals was named a three-electron subspace because it described only the correlation effects of the 3 valence electrons. A subspace spanned by all the CSF with fully occupied core orbitals was named a 19-electron subspace, because it described only correlation effects of the 19 outermost electrons. A null space was named a zero-electron space.

A series of four CI claculations was performed to examine the importance of various n-particle subspaces. The n-particle space of each calculation may be denoted by a triplet of indices (i, s, d) corresponding to the number of electrons correlated in the internal, singly excited, and doubly excited subspaces. For example, (0, 0, 0) denotes a null space, and (3, 3, 3) denotes the union of the three-electron part of the three n-particle spaces. In this notation our CI calculations are given by (3, 3, 0), (19, 19, 0), (3, 3, 3), and (19, 19, 3). The dimensions of these CI calculations for both symmetries are 65, 871, 1131, and 1937, respectively. The first two are known as first-order CI[6] calculations. They include internal, semi-internal, and polarization effects.[7] The third calculation includes the most important external, valence correlation[7] effects. The last calculation includes internal and semi-internal correlation effects of the 19 outermost electrons and the external correlation effects of the 3 valence electrons.

B. Potential curves

The SCF and CI energies for the ${}^2\Sigma_u^+$ and ${}^2\Sigma_g^+$ states are given in Tables II and III, respectively. The CI (19, 19, 3) potential curves, our best result, are also shown in Fig. 1. For ease of comparison, the calculated energies are given as interaction energies, $E_{\text{int}}(R) = E(R) - E(\infty)$. The asymptotic total energies $E(\infty)$ are also tabulated.

The minimum in each of the ${}^2\Sigma_u^+$ potential curves was obtained by polynomial interpolation. The result was used to obtain the dissociation energy of Ca_2^+. The long-range parts of these potential curves were also parametrized to yield C_4 and C_6 coefficients. The results are summarized in Table IV. The long-range parts of both ${}^2\Sigma_u^+$ and ${}^2\Sigma_g^+$, CI (19, 19, 3) potential curves are characterized by a dipole polarizability of $170.4a_0^3$, which is in good agreement with the experimental value[8] of $(169 \pm 17)a_0^3$, but above the more reliable theoretical value of $(154 \pm 3)a_0^3$ by Reinsch and Meyer.[9]

Vibrational wave functions were calculated for the ${}^2\Sigma_u^+$ state using the CI (19, 19, 3) potential curve. Spectroscopic constants obtained from the vibrational energy levels are given in Table V.

A comparison of the calculated potential curves gives some indication of their accuracy. The differences between the CI potential curves of each symmetry are quite small. This shows that inter-

TABLE II. Interaction potential energies for the $X^2\Sigma_u^+$ state of Ca_2^+, $E(R)-E(\infty)$ (units of 10^{-3} hartrees).

$R(a_0)$	SCF	CI (3,3,0)	CI (19,19,0)	CI (3,3,3)	CI (19,19,3)
4.0	232.419	229.167	227.137	218.496	216.774
5.0	70.799	66.431	65.900	59.356	58.902
6.0	−6.371	−11.516	−11.645	−14.102	−14.246
6.5	−22.235	−27.978	−28.034	−29.036	−29.122
7.0	−29.615	−36.017	−36.034	−35.960	−36.015
7.5	−31.828	−38.825	−38.823	−38.001	−38.070
7.75	−31.716	−38.953	−38.946	−37.850	−37.884
8.0	−31.065	−38.490	−38.480	−37.165	−37.197
8.5	−28.726	−36.346	−36.335	−34.714	−34.745
9.0	−25.677	−33.237	−33.230	−31.434	−31.466
10.0	−19.285	−26.067	−26.064	−24.170	−24.206
12.0	−9.594	−13.718	−13.714	−12.153	−12.186
15.0	−3.028	−4.479	−4.477	−3.746	−3.761
20.0	−0.563	−0.849	−0.850	−0.721	−0.723
30.0	−0.091	−0.115	−0.117	−0.112	−0.112
		Asymptotic total energies (hartrees)			
$E(\infty)$	−1353.323353	−1353.327942	−1353.329999	−1353.355860	−1353.357717

TABLE III. Interaction potential energies for the $X^2\Sigma_g^+$ state of Ca_2^+, $E(R)-E(\infty)$ (units of 10^{-3} hartrees).

$R(a_0)$	SCF	CI (3,3,0)	CI (19,19,0)	CI (3,3,3)	CI (19,19,3)
4.0	340.451	223.120	223.265	243.370	243.313
5.0	174.555	122.485	123.057	124.982	125.460
6.0	86.808	49.000	48.773	48.848	48.486
6.5	62.469	28.689	28.572	28.642	28.424
7.0	45.969	16.285	16.294	16.244	16.197
7.5	34.668	8.610	8.758	8.759	8.870
7.75	30.386	5.891	6.110	6.269	6.448
8.0	26.789	3.685	3.973	4.394	4.632
8.5	21.146	0.442	0.851	2.016	2.340
9.0	16.951	−1.588	−1.088	0.875	1.244
10.0	11.076	−3.069	−2.499	0.395	0.748
12.0	4.332	−1.311	−0.942	0.429	0.598
15.0	0.530	−0.352	−0.290	−0.414	−0.380
20.0	−0.297	−0.457	−0.457	−0.480	−0.480
30.0	−0.088	−0.111	−0.113	−0.109	−0.110
		Asymptotic total energies (hartrees)			
$E(\infty)$	−1353.323353	−1353.327942	−1353.329999	−1353.355860	−1353.357717

TABLE IV. Parametrized fits to the average of the $^2\Sigma_u^+$ and $^2\Sigma_g^+$ long-range potentials and to the $^2\Sigma_u^+$ potential at its equilibrium internuclear separation.

Calculation	C_4 (hartrees^4)	C_6 (hartrees^6)	$R_e(a_0)$	D_e (eV)
SCF	−75.9	+2860	7.58	0.867
CI (3,3,0)	−81.4	−9190	7.67	1.061
CI (19,19,0)	−83.8	−8300	7.67	1.061
CI (3,3,3)	−84.1	−4760	7.56	1.035
CI (19,19,3)	−85.2	−4420	7.55	1.036

TABLE V. Spectroscopic constants for the $^2\Sigma_u^+$ potential.

V	G_v (cm^{-1})	B_v (cm^{-1})	D_v (cm^{-1})[a]
0	0.00	0.053	4.13(−6)
1	117.93	0.052	4.20(−6)
2	234.42	0.052	4.16(−6)
3	350.15	0.052	4.16(−6)
4	465.09	0.051	4.20(−6)
5	579.17	0.051	4.20(−6)
	$\omega_e = 119$ cm^{-1}	$B_e = 0.0526$ cm^{-1}	

[a] Powers of 10 are given in parentheses.

nal and semi-internal correlation effects of the inner-shell electrons, as well as the external correlation effects of the valence electrons, have little influence on the shape of the potential curves. From this it seems safe to infer that the external correlation effects of the inner orbitals and all the correlation effects of the core electrons are negligible. The small contribution of the external correlation effects also suggests that higher than double excitations would have very little effect on the potential curves. Inclusion of these higher than double excitations would result in a more attractive, or less repulsive interaction potential, but the change should be small compared to the effects of the double excitations. On the basis of the above analysis we conservatively estimate that our CI (19, 19, 3) potential curves have an overall accuracy of ±10%. Our best estimates for the bond length and dissociation energy of Ca_2^+ ($^2\Sigma_u^+$) are $R_e = (7.55 \pm 0.05)a_0$ and $D_e = 1.04 \pm 0.1$ eV, respectively.

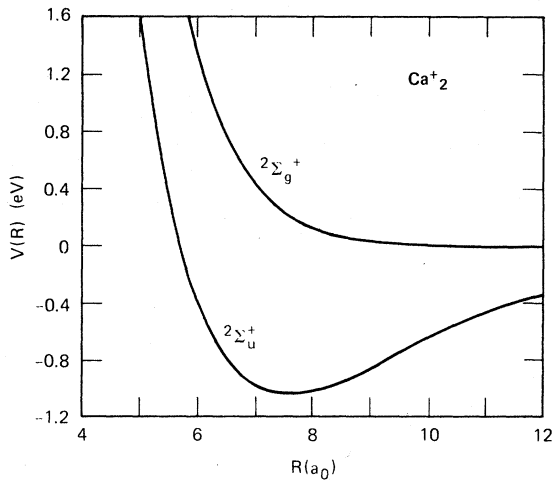

FIG. 1. *Ab initio* potential energy curves for the ground state of Ca_2^+ from the CI (19,19,3) calculation.

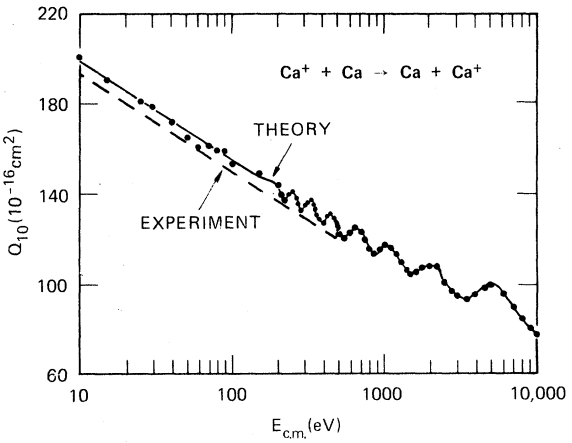

FIG. 2. Comparison of the calculated resonant charge-transfer total cross sections (points and line) to the experimental data of Panev *et al.* from Ref. 11 (dashed line). At energies below 200 eV, the calculated oscillation frequency (proportional to v^{-1}) becomes so rapid that we have represented the averaged cross section by a line.

III. SCATTERING CROSS SECTIONS

A. Resonant charge-transfer total cross sections

The *ab initio* potentials from the CI (19, 19, 3) calculation have been used to calculate the resonant charge-transfer total cross sections for the reaction

$$Ca^+ + Ca \rightarrow Ca + Ca^+. \tag{2}$$

At center-of-mass collision energies, $E_{c.m.} = 10$–10 000 eV, it is valid to use the straight-line impact parameter formulation[10] where the cross section Q_{10} is given in terms of the difference in phase shifts $\Delta\delta$ as a function of impact parameter b for scattering on the gerade and ungerade potential curves:

$$Q_{10} = 2\pi \int_0^\infty db\, b \sin^2\Delta\delta(b). \tag{3}$$

In the straight-line impact parameter formulation, the phase shift difference is directly related to the difference in potential energies $\Delta V(R)$ between the $^2\Sigma_u^+$ and $^2\Sigma_g^+$ molecular states by the integral

$$\Delta\delta(b) = -\frac{1}{\hbar v}\int_b^\infty \frac{dR R \Delta V(R)}{(R^2 - b^2)^{1/2}}, \tag{4}$$

where v is the relative asymptotic velocity of the collision.

Figure 2 presents a comparison of the total cross sections calculated using Eqs. (3) and (4) and the experimental cross sections of Panev *et al.*[11] The theoretical and experimental cross sec-

tions differ by less than 5%. Such agreement was unexpected since the absolute values of the experimental cross sections were estimated to be uncertain by ±30%. The experimental relative cross sections, however, have a much lower uncertainty of ±2% at collision energies above 50 eV and are also found to be in good agreement with the theoretical values.

Rutherford *et al.*[12] have also measured these cross sections in the energy range 15–250 eV with an estimated uncertainty of ±30%–60%. Their values are found to be approximately a factor of 2.3 larger than the theoretical cross sections. However, the energy dependence of these experimental values are in reasonable agreement with theory.

Sinha and Bardsley[1] have calculated two sets of cross sections for reaction (2) that depend on the normalization constant used for the exchange splitting. The *ab initio* potentials presented here indicate that of the two normalization constants used, $q = 1.0$ and 1.5, the 1.5 value is most appropriate for the $Ca^+ + Ca$ reaction.

To obtain an accuracy estimate of the theoretical cross sections presented in Fig. 2, we have also calculated the cross sections using the SCF and first-order CI potentials. Rather than calculating the cross sections numerically, we have used a method described previously[13] for an exponential splitting between the gerade and ungerade potentials at large separations. If the difference potential can be represented by the functional form

$$\Delta V(R) = A \exp(-BR), \tag{5}$$

then the phase shift difference for (4) is given by

$$\Delta\delta(b) = -(A/\hbar v) b K_1(Bb), \tag{6}$$

where K_1 is a modified Bessel function of the second kind. The cross section is then determined analytically, with an accuracy of ~5%, by the use of the relationship given by Firsov,[14]

$$Q = \tfrac{1}{2}\pi b_f^2, \tag{7}$$

where b_f is the impact parameter for which

$$|\Delta\delta(b_f)| = 1/\pi. \tag{8}$$

Equation (6) can be further simplified if $Bb \gg 2$ by the use of the asymptotic expansion[15]

$$K_1(Bb) \approx 1.2533 (Bb)^{-1/2} \exp(-Bb). \tag{9}$$

The cross section is then obtained by using Eq. (7) and solving for b_f in the formula

$$b_f^{1/2} \exp(-Bb_f) = \hbar v B^{1/2}/3.9374A. \tag{10}$$

For the Ca_2^+ system, $\Delta V(R)$ is exponential for $R \gtrsim 12a_0$, and Bb of Eq. (9) ranges from ~10 at 10 eV to ~6 at 10 000 eV. Hence, the use of Eqs. (7) and (10) is valid for the comparisons of the total cross sections obtained using the potentials calculated with various degrees of sophistication. We find that the SCF and the CI (3, 3, 3) and CI (19, 19, 3) potentials yield cross sections that are almost identical. The first-order CI potentials CI (3, 3, 0) and CI (19, 19, 0), on the other hand, yield cross sections that are ~10% larger than the previous two sets of potentials. Hence, it appears that the calculated cross sections are reasonably converged on the true values and have a probable accuracy of ±10%. A curve fit of the monotonically decreasing portion of the calculated cross section yields:

$$Q^{1/2}(\text{Å}) = 15.67 - 3.276 \log_{10} E_{\text{c.m.}}\,(\text{eV}). \tag{11}$$

A complication is that inelastic processes may further increase the total cross sections. Calculations by McMillan[16] on the Li_2^+ system indicate that the magnitude of the calculated total cross sections is only slightly changed by the inclusion of inelastic events. However, the oscillatory structure is changed appreciably. Hence, the oscillations observed on the calculated cross sections of Fig. 2 have a high uncertainty level.

B. Differential scattering cross sections

It is also of interest to estimate the position of the rainbow scattering angle for collisions of Ca^+ on Ca. A classical description of this process is particularly easy to apply if the attractive state of a system can be accurately described by an analytical potential form.

For the $^2\Sigma_u^+$ state of Ca_2^+, the Morse potential form is applicable:

$$V(R) = D_e\{\exp[2\alpha(1 - R/R_e)] - 2\exp[\alpha(1 - R/R_e)]\}. \tag{12}$$

We have used the CI (19, 19, 3) potential in the rainbow calculation with $D_e = 1.036$ eV, $R_e = 7.55a_0$, and $\alpha = 2.836$. The deflection angle for scattering from an exponential potential of the form given by Eq. (5) is related to the impact parameter and the center-of-mass collision energy by[17]

$$E\theta = ABbK_0(Bb), \tag{13}$$

where K_0 is a modified Bessel function of the second kind. Hence, for scattering on the Morse potential given by (12):

$$E\theta(\text{eV deg}) = 114.59 D_e(\text{eV}) \times \beta e^{\alpha}[e^{\alpha} K_0(2\beta) - K_0(\beta)], \tag{14}$$

where

$$\beta = \alpha b/R_e. \tag{15}$$

The classical rainbow scattering angle is then the minimum value of Eq. (14).

Inserting the Morse potential parameters given above into Eq. (14) and solving for the minimum value, we find a classical rainbow angle at $E\theta_R = 90$ eV deg. The impact parameter corresponding to the rainbow scattering is $b = 8.8a_0$. As a check of the above classical calculation, we have also performed a semiclassical two-state calculation of the differential scattering using standard methods.[18] For a collision energy of 5 eV, the computed rainbow angle is 87 eV deg, in very good agreement with the classical result.

C. Ionization cross sections

Recently, Armstrong *et al.*[19] have performed some interesting experiments using a dye laser to pump Rydberg states of Ca. These authors observed that when the two-photon energy was within 7300 cm^{-1} of the atomic ionization limit, ionization occurred with a rate proportional to the square of the laser intensity. This type of behavior may be explained in terms of the Hornbeck-Molnar[20] ionization reaction:

$$Ca^{**} + Ca \rightarrow Ca_2^+ + e^- \quad \text{or} \quad Ca^+ + Ca + e^- . \tag{16}$$

To estimate the cross sections for process (16), we have assumed that during the ionizing collision the neutral particles follow potential curves that diabatically cross into the continuum of the ionic state where electron ejection is known to occur with almost unit probability at low collision energies.[21] The ionization cross section is then simply given by

$$Q_{\text{ion}} = \pi P R_*^2 , \tag{17}$$

where R_* is the crossing distance and P is the probability that the particles follow the diabatic potentials into the continuum.

For collisions between high-lying Rydberg states and their parent ground state, it is possible to estimate R_* by solving

$$\alpha_d / 2R_*^4 = 0.5/n^2 . \tag{18}$$

In Eq. (18), we have assumed that the long-range portion of the ionic potential is determined by the point charge-induced dipole interaction, which is given in terms of the dipole polarizability α_d of the neutral partner. We have not included the exchange interaction since it is exponentially decreasing and negligible compared to the R^{-4} interaction in the internuclear region of interest. The Rydberg state interaction is assumed to be constant and equal to its ionization energy, which to first order is simply given by $0.5/n^2$, where n is the principle electronic quantum number of the Rydberg atom. We could include the quantum defect in the ionization energy of the Rydberg atom; however, the approximate nature of Eqs. (17) and (18) does not warrant its inclusion.

If Eqs. (17) and (18) are combined, the ionization cross section

$$Q_{\text{ion}} = \pi P n \alpha_d^{1/2} , \tag{19}$$

is found to increase linearly with n and to depend on the square root of the dipole polarizability of the neutral atom formed.

The probability P of Eq. (19) for the states crossing into the continuum is more difficult to estimate. However, for Ca**+Ca collisions, we may relate the shape of the Rydberg potentials to that of the attractive (core) $4s\sigma_g^2 4s\sigma_u\ ^2\Sigma_u^+$ and repulsive (core)$4s\sigma_g 4s\sigma_u^2\ ^2\Sigma_g^+$ ion molecular states. For collisions of Ca**$(4s\,ns)$ with Ca, the $^1\Sigma_u$ and $^3\Sigma_u$ states formed will have the basic configuration (core)$4s\sigma_g^2 4s\sigma_u ns\sigma_g$. Thus, because of the diffuse nature of the Rydberg electron, these states will be approximately parallel to, and below, the attractive $^2\Sigma_u^+$ ion state and will not cross into the continuum. However, the $^1\Sigma_g$ and $^3\Sigma_g$ molecular Rydberg states will have the configuration (core)$4s\sigma_g 4s\sigma_u^2 ns\sigma_g$, which is similar to the repulsive $^2\Sigma_g^+$ ionic state, and thus they will cross into the continuum. Hence, we predict a 50% probability of crossing into the continuum for Rydberg Ca**$(4s\,ns)$+Ca collisions. The collision mechanism is a two-electron process, similar to that found for He*+He collisions,[22] that involves the ejection of an s-wave electron from the $4s\sigma_u$ orbital and the transition of the Rydberg $ns\sigma_g$ electron to the $4s\sigma_g$ orbital:

$$(\text{core})4s\sigma_g 4s\sigma_u^2 ns\sigma_g \rightarrow (\text{core})4s\sigma_g^2 4s\sigma_u + e^- . \tag{20}$$

Armstrong *et al.*[19] also observed ionization of Rydberg Ca**$(4s\,nd)$. As for the Ca**$(4s\,ns)$ case discussed above, the ungerade molecular states will lie below the $^2\Sigma_u^+$ ionic state and will not cross into the continuum. The gerade states, however, will cross into the continuum and consist of $^1\Sigma_g$ and $^3\Sigma_g$-(core)$4s\sigma_g 4s\sigma_u^2 nd\sigma_g$, $^1\Pi_g$ and $^3\Pi_g$-(core)$4s\sigma_g 4s\sigma_u^2 nd\sigma_g$ and $^1\Delta_g$ and $^3\Delta_g$-(core)$4s\sigma_g 4s\sigma_u^2 nd\delta_g$. For thermal energy collisions we argue that only the $^1\Sigma_g$ and $^3\Sigma_g$ will couple to the continuum and give rise to ionization via the two-electron process:

$$(\text{core})4s\sigma_g 4s\sigma_u^2 nd\sigma_g \rightarrow (\text{core})4s\sigma_g^2 4s\sigma_u + e , \tag{21}$$

where the electron in the $4s\sigma_u$ orbital is ejected and the Rydberg electron in the $nd\sigma_g$ orbital transfers to the $4s\sigma_g$ orbital. The Π_g and Δ_g molecular states would require the conversion of a $4s\sigma_u$ orbital to a $4s\sigma_g$ orbital and the ejection of a p-

d-wave electron, a process requiring more kinetic energy than is available in a thermal-energy collision. Hence, we predict only a 10% probability for electron ejection for Ca**($4s\,nd$) which is a factor of 5 lower than that for the Ca**($4s\,ns$) system discussed above.

For both the Ca**($4s\,ns$) and Ca**($4s\,nd$) systems it is possible there may be a slight added contribution to the ionization cross section from the trajectories that follow the attractive potentials. Since the potential well depth is so much larger than the collision energy, orbiting is possible for selected collisional angular orbital momentum quantum values. These orbiting collisions will have an increased probability for ionization due to the better overlap between the neutral particle and continuum wave functions. However, the number of orbiting collisions at a given collision energy is small. Therefore, within the approximate formulism for chemi-ionization presented above, we may neglect this orbiting contribution.

For thermal-energy collisions, the probability for electron ejection, and hence the cross section, must be zero when the Rydberg level lies below the minimum in the potential well for the molecular ion. For the Ca_2^+ system, our calculated potential well for the $^2\Sigma_u^+$ states lies 40 950 cm^{-1} above the separated atom limit of two ground-state Ca atoms. Therefore, the ionization will be zero until excited states of Ca are produced above this limit. The observations of Armstrong *et al.*[19] support this conclusion; collisional ionization was not observed when they pumped the $4p^2\,^1D_2$ state of Ca at 40 720 cm^{-1}, but it was observed for the next higher $^1D_2$ state at 42 919 cm^{-1}.

We have examined collisions of Ca**($4s\,20s$) and Ca**($4s\,20d$) with Ca as representative cross sections and rates for ionization. Using Eq. (19) and the calculated dipole polarizability for Ca, we estimate a chemi-ionization cross section of 1×10^{-14} cm^2 for Ca**($4s\,20s$) and 2×10^{-15} cm^2 for Ca**($4s\,20d$). These cross sections correspond to thermal-energy reaction rates of 5×10^{-10} and 1×10^{-10} cm^3/sec, respectively. Using these rates, we calculate that the lifetime of Ca**($4s\,20s$) or Ca**($4s\,20d$) in a 0.1-Torr pressure of Ca atom will be on the order of 1 μsec, which agrees with the observations of Armstrong *et al.*[19] that the lifetimes must be less than 1 msec.

Equation (19) is sufficiently general that it may be used for ionizing collisions of high-lying excited states with their parent ground states. An interesting example is the reaction

$$Ar^* + Ar \rightarrow Ar_2^+ + e^- \quad \text{or} \quad Ar^+ + Ar + e^-. \tag{22}$$

Using a dipole polarizability[23] of $11.1a_0^3$ for Ar, we estimate chemi-ionization rates approximately a factor of 4 lower than for Ca** + Ca collisions. Hence, we would estimate a rate of $\sim10^{-10}$ cm^3/sec, along with only a linear dependence on the electronic excitation level n. Kinetic studies confirm that the reaction rate for (20) is of the order 10^{-10}–10^{-9} cm^3/sec and is approximately independent of the level of excitation as long as the ionic state is accessible to a thermal-energy collision.[24] Hence, we conclude that our predicted ionization rates for Ca** + Ca are good order of magnitude estimates.

IV. SUMMARY

Ab initio potential energy curves have been presented for the ground $^2\Sigma_u^+$ and $^2\Sigma_g^+$ states of Ca_2^+. Our estimated bond length and dissociation energy for the $^2\Sigma_u^+$ state are $R_e = (7.55 \pm 0.05)a_0$ and $D_e = 1.04 \pm 0.1$ eV, respectively. From the $^2\Sigma_u^+$ potential well, we predict a rainbow scattering angle of 90 eV deg for the elastic or charge-exchange differential cross sections. Total charge-exchange cross sections were also calculated over the collision energy range of 10–10 000 eV and were found to be in very good agreement as to magnitude and energy dependence with the measurements of Panev *et al.*[11] Thermal-energy cross sections and reaction rates were estimated for chemi-ionization collisions of Rydberg Ca** atoms with ground-state Ca. Ionization cross sections on the order of 10^{-14} cm^2 and reaction rates of 10^{-10} cm^3/sec are predicted along with a linear dependence on the principal quantum number. These predictions appear reasonable considering the analogy with Ar* + Ar ionization rates.

ACKNOWLEDGMENTS

This work was performed under a joint study contract between SRI International and IBM. The work of one of the authors (R.E.O.) was also supported by the Air Force Office of Scientific Research under Contract No. F44620-75-C-0073.

[1] S. Sinha and J. N. Bardsley, Phys. Rev. A 14, 104 (1976).
[2] K. Sakurai and H. P. Broida, J. Chem. Phys. 65, 1138 (1976).
[3] W. J. Balfour and R. F. Whitlock, Can. J. Phys. 53, 472 (1975).
[4] W. J. Stevens and M. Krauss, J. Chem. Phys. 67, 1977 (1977).

[5]E. Clementi and C. Roetti, At. Data Nucl. Data Tables 14, 1977 (1974).
[6]H. F. Schaefer III, R. H. Klemm, and F. E. Harris, Phys. Rev. 181, 137 (1969).
[7]H. Silverstone and O. Sinanoglu, J. Chem. Phys. 44, 1899 (1966).
[8]T. M. Miller and B. Bederson, Phys. Rev. A 14, 1572 (1976).
[9]E. A. Reinsch and W. Meyer, Phys. Rev. A 14, 915 (1976).
[10]D. R. Bates and R. McCarroll, Adv. Phys. 11, 39 (1962).
[11]G. S. Panev, A. N. Zavilopulo, I. P. Zapesochnyi, and O. B. Shpenik, Zh. Eksp. Teor. Fiz. 67, 47 (1974) [Sov. Phys. JETP 40, 23 (1975)].
[12]J. A. Rutherford, R. F. Mathis, B. R. Turner, and D. A. Vroom, J. Chem. Phys. 57, 3087 (1972).
[13]R. E. Olson, Phys. Rev. 187, 153 (1969).
[14]O. Firsov, Zh. Eksp. Teor. Fiz. 21, 1001 (1951).
[15]M. Abramowitz and I. A. Stegun, *Handbook of Mathematical Functions* NBS Applied Mathematics Series 55 (U.S. GPO, Washington, D.C., 1967), p. 379.
[16]W. L. McMillan, Phys. Rev. A 4, 69 (1971).
[17]Chr. Lehmann and G. Leibfried, Z. Phys. 172, 465 (1963).
[18]R. E. Olson and C. R. Mueller, J. Chem. Phys. 46, 3810 (1967).
[19]J. A. Armstrong, P. Esherick, and J. J. Wynne, Phys. Rev. A 15, 180 (1977).
[20]J. A. Hornbeck and J. P. Molnar, Phys. Rev. 84, 621 (1951).
[21]S. K. Lam, J. B. Delos, R. L. Champion, and L. D. Doverspike, Phys. Rev. A 9, 1828 (1974).
[22]K. T. Gillen, J. R. Peterson, and R. E. Olson, Phys. Rev. A 15, 527 (1977).
[23]R. R. Teachout and R. T. Pack, At. Data 3, 195 (1971).
[24]N. T. Holcombe and F. W. Lampe, J. Chem. Phys. 56, 1127 (1972).